Reprint from

"PLASMA PHYSICS
AND CONTROLLED
NUCLEAR FUSION RESEARCH 1982"

VOL. I

INTERNATIONAL ATOMIC ENERGY AGENCY
VIENNA, 1983

EXPERIMENTAL MODELLING OF LASER-PLASMA INTERACTION PHYSICS*

C.E. CLAYTON, H.E. HUEY, C. PAWLEY,
A.Y. LEE, F.F. CHEN, C. JOSHI,
N.C. LUHMANN, Jr.
University of California,
Los Angeles, California,
United States of America

Abstract

EXPERIMENTAL MODELLING OF LASER-PLASMA INTERACTION PHYSICS.

The authors have performed two series of experiments, one using a CO_2 laser pump, and the other a high-power microwave pump, to elucidate the details of laser-plasma interaction phenomena occurring in both underdense pellet coronas and the vicinity of the critical layer. The work includes the study of SBS saturation, the saturation of ion waves produced by optical mixing, resonant self-focusing due to optical mixing generation of electron plasma waves, filamentation and the saturation of resonance-absorption-produced electron plasma waves.

1. Stimulated Brillouin Scattering

1.1 CO_2 Laser Driver

In earlier work we have confirmed the exponential growth of SBS from thermal noise,[1] observed Brillouin sidescattering,[2] measured backscatter saturation levels,[3] and checked its dependence on focusing f-number and target Z.[4] However, the physics of the interaction is more richly revealed by studying the SBS ion wave directly.[5] In our SBS experiment, the SBS backscatter wave grows and saturates at a reflectivity of about 5% at an imput CO_2 laser intensity of 3×10^{11} W/cm^2. If the ion wave amplitude is assumed to be uniform over the interaction length L then the reflectivity R is given by the usual Bragg formula as $R = (\pi n_o L\tilde{n}/Zn_c\lambda_o n_o)^2$, where $\tilde{n}/n_o$ is the density fluctuation level normalized to the electron density. However, for our experimental conditions, the SBS instability is in the convective regime,[6] which means that the ion wave amplitude varies greatly over the interaction length L. In the strong damping case, $ZT_e/3T_i = 0(1)$, the ion wave amplitude decreases exponentially with distance x from saturation level to noise level in the direction of the laser

* Work supported by Lawrence Livermore National Laboratory Inertial Fusion Program and DOE-DEAS08-81DP 40166, NSF ECS 80-03558.

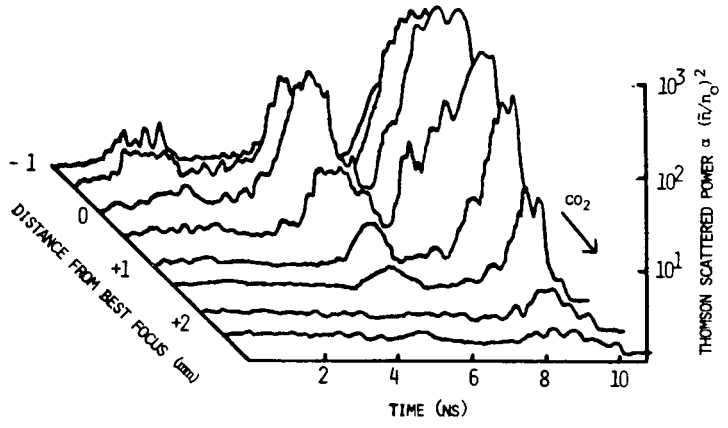

FIG.1. Space and time evolution of the SBS-driven ion acoustic wave obtained by collective Thomson scattering.

beam; $\tilde{n}(x)/n_o = (NR^{\frac{1}{2}}/\beta L)\exp(-N\lambda/2L)$ where $\beta = (n_o/n_c)(\pi/\lambda_o)$ and N is the number of e-foldings growth. We have experimentally verified the nature of the SBS instability (whether absolute of convective) by employing collective Thomson scattering to probe the behaviour of the ion wave.

For backscatter with $n << n_c$, the propagation constant of the ion wave is fixed at $\underline{k}_s = 2\underline{k}_o = 11900\ cm^{-1}$. The Thomson scattering relation $|\underline{k}_s| = 2\underline{k}_{probe}\sin(\theta/2)$ leads to the scattering angle θ of $\pm 7.5^o$ for $\underline{k} = \underline{k}_{probe} \pm \underline{k}_s$. Also since $|\underline{k}_s| << |\underline{k}_{probe}|$, $|\underline{k}| \simeq |\underline{k}_{probe}|$ and the probe ruby beam comes in at an angle of 86^o to the CO_2 laser axis. The scattering parameter $\alpha = 1/k_s\lambda_D$ is about 10 for $n \simeq 2\times10^{17}\ cm^{-3}$, $T_e \simeq 20$ eV. The probe beam is an $\simeq$200-mJ, 30-ns ruby laser pulse focused using an f/20 lens. Light scattered in the forward direction at 7.5^o is collected, dispersed by a grating, and recorded by an optical multi-channel analyzer (OMA). The spectrograph-OMA resolution of 0.05 Å per channel is sufficient to allow the acoustic shifts to be measured. The scattered light is clearly red- or blue-shifted (depending on whether θ is - or + 7.5^o), corresponding to ω_s = 9-12 GHz, in agreement with the measured SBS redshift. The $\underline{k}_s$ spectrum was checked by varying the scattered angle θ. The scattered ruby light was sharply collimated within $1/4^o$ of 7.5^o (FWHM), showing that the acoustic wave is sharply collimated along $\underline{k}_o$, in agreement with observations of optical ray retracing of SBS. There is a reasonable correlation between the level of Thomson scattered power and SBS reflectivity. To probe for the axial variation of the ion wave amplitude, a cylindrical lens was used to focus the ruby to a line focus overlapping the ion wave. The Thomson scattered light at the $\underline{k}$-matching angle was imaged with unity magnificaton onto

the slit of the streak camera. Spatial variations in the ion wave amplitude showed up as variations in scattered power across the slit. This image of the ion wave was streaked in time resulting in data such as shown in Fig. 1. The ion wave was found to be hundreds of wavelengths long with a single peak at the CO_2 laser end. The ion wave was seen to come in bursts in time (behaviour not as yet explained) but was stationary in space, nonlinearly increasing in amplitude towards the laser, in agreement with the notion of highly Landau-damped ion waves which do not convect appreciably in the forward direction.

The level of the saturated SBS reflectivity implies that the ion wave saturates at an amplitude of a few percent. To test whether harmonic generation is a possible saturation mechanism we scattered at 15° to see the second harmonic at $\underline{k}_s = 4\underline{k}_o$. This indeed exists but its dependence on CO_2 laser power and its spatial amplitude distribution suggest that the harmonic amplitude is linearly proportional to the amplitude of the fundamental regardless of the amplitude of the fundamental. This does not fit the picture of harmonic generation as a saturation mechanism.

1.2 Microwave Driver

We have previously reported the observation of SBS growth in microwave interaction with an underdense ($n = 0.1\ n_c$) plasma, [7] the saturation of the reflectivity R at ≃5% due to ion tail heating and electron main body heating, [8] and finite bandwidth control of the reflectivity. [8] Herein, we report further studies of SBS saturation, observation of multiple red-shifted peaks in the reflected spectrum spaced at the sound frequency ω_s, the evolution to a turbulent spectrum, and the identification of ion acoustic waves.

The experiments were performed in an unmagnetized plasma ($n/n_c = 0.1$, $n \simeq 1.4\times10^{10}$ cm^{-3}, $T_e \simeq 2$-3 eV, $T_e/T_i \simeq 10$-15, and $L_n = n/(dn/dx)^{-1} \simeq 2.5$ m). The 3.3 GHz ($\lambda_o \simeq 11$ cm) microwave source produced up to 1 MW ($v_o/v_{te} \simeq 1$) with a miximum pulse duration $\tau = 47$ μm ($\omega_s\tau \simeq 100$ for an H_3^+ plasma) and resulted in an effective interaction length of ≃70-120 cm. The residual reflectivity r of the back chamber wall into the 17 dB gain input horn together with rapid turn-on of the pump gives rise to a transient density perturbation given approximately by [7, 8] $\tilde{n}/n_o = r^{\frac{1}{2}}(v_o/v_e)^2 (1 - e^{\omega t} \cos \omega_s t) \cos 2\underline{k}_o x$ which can be decomposed into a steady zero frequency density perturbation together with forward and backward propagation ion waves. The forward propagation wave serves as an enhanced noise level from which SBS grows. [7, 8]

For r = 1%, the SBS reflectivity R saturates at ≃ 3.5% as shown in Fig. 2. Density profile modification (< 10%) was not a factor in the saturation nor was ion acoustic harmonic generation (harmonic content < 10% of the fundamental). Experimentally, both

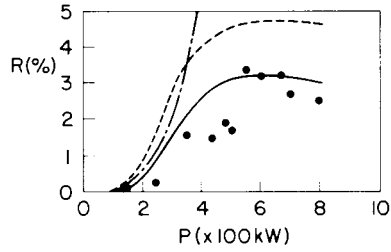

FIG.2. Comparison of power dependence of measured SBS reflectivity (dots) versus numerical predictions. The solid curve represents the complete calculation. The – – – – curve neglects ion tail heating, while the – · – · – · – curve neglects electron bremsstrahlung heating.

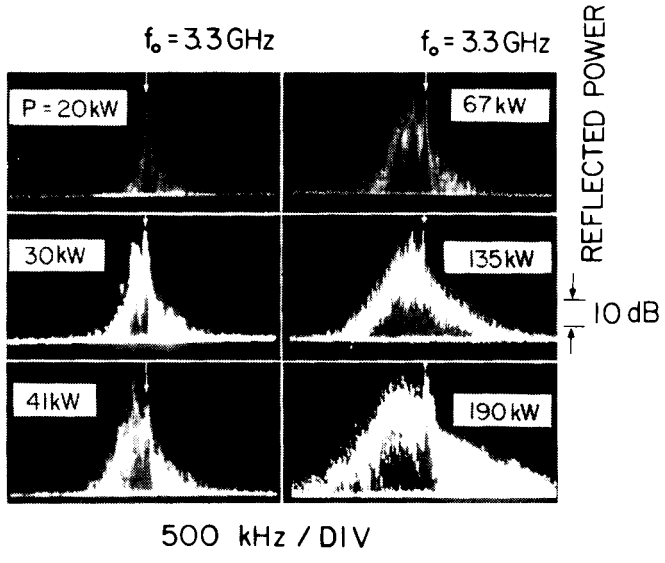

FIG.3. Reflected electromagnetic wave spectrum for various input power levels with an initial chamber wall reflectivity r = 3%.

ion tail heating and electron main body heating (due to inverse bremsstrahlung absorption on the neutrals) are observed. The relative importance (in saturation) of each of these effects was studied numerically, as shown by the curves in Fig. 2; neither effect alone is sufficient to completely account for the observed SBS saturation. Furthermore, Fig. 2 shows that ion tail heating is the dominant saturation mechanism.

When the initial chamber wall reflectivity is increased from $\simeq$ 1% to $\simeq$ 3%, additional phenomena are observed. For example,

Fig. 3 shows the change in the spectrum of the reflected signal in He plasma ($\omega_s/2\pi$ = 170 kHz) as the input power is increased. Each red-shifted peak is spaced at the acoustic frequency and there appears to be a threshold for the appearance of each peak. Often the $2\omega_s$ red-shifted peak can be larger than the ω_s peak. Note that multiple scattering from the forward and backward propagating ion waves as well as chamber reflections would result in a cascade of red-shifted peaks without separate threshold and with decreasing amplitude. In addition, standing ion wave harmonics ($2\omega_s$, $4\underline{k}_o$) were observed in the presence of an ($\omega_o - 2\omega_s$) peak. This observation can be explained by considering the development of spatial harmonics of the incident and reflected electromagnetic wave as required by Floquet's Theorem due to the periodic spatial modulation of the plasma dielectric function. These spatial harmonics in turn create standing density perturbations of higher order (i.e. $4\underline{k}_o$). Scattering of an electromagnetic wave spatial harmonic (i.e. ω_o, $3\underline{k}_o$) with an ion wave harmonic (i.e. $2\omega_s$, $4\underline{k}_o$) can lead to the observed spectra. Figure 3 also indicates that at higher power the reflected spectrum becomes turbulent. Ion energy analyzer measurements indicate that a large ion tail distribution also develops in both directions suggesting the occurrence of a two-stream instability.

2. Optical Mixing Studies

Two electromagnetic waves ($\omega_1,\underline{k}_1$) and ($\omega_2,\underline{k}_2$) occupying the same volume give rise to a density modulation due to the ponderomotive force F_{NL} associated with the beat wave ($\Delta\omega,\Delta\underline{k}$) where $\Delta\omega = \omega_1 \pm \omega_2$ and $\Delta\underline{k} = \underline{k}_1 \pm \underline{k}_2$. The resultant density fluctuations can become appreciable whenever $\Delta\omega$ and $\Delta\underline{k}$ satisfy the plasma dispersion relation $\varepsilon(\Delta\omega,\Delta\underline{k}) = 0$. The process is commonly referred to as optical mixing.

2.1 Ion Wave Saturation Studies

By adding a second microwave source to the experiment described above, we have studied the optical mixing of two antiparallel propagating electromagnetic waves. The difference frequency between the two sources can be accurately set (and maintained) to within ±100 Hz over the range from zero through the appropriate ion acoustic frequency and up to the electron plasma frequency. By setting $\Delta\omega = \omega_s$, we have studied the saturation of SBS ion waves. This also models the actual laser interaction in which imperfect absorption of the laser light can lead to the Doppler shifted light reflected from the moving critical layer beating with the incoming laser light. The microwave results can be summarized as follows. At low intensities ($v_o/v_{te} = e(E_1E_2)^{1/2}/m\Delta\omega v_{te} \lesssim 0.08$) the predictions of optical mixing were verified where the ion wave reaches a steady state amplitude limited by

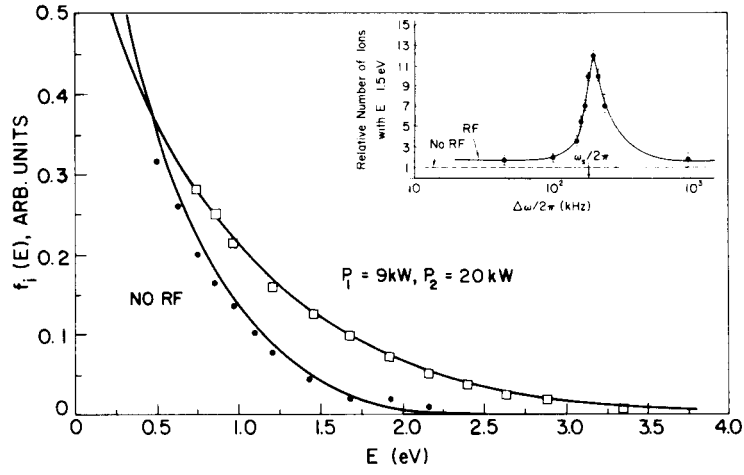

FIG.4. Ion tail distribution function with and without RF. The inset shows the relative number of ions with E > 1.5 eV as a function of the microwave difference frequency.

collisions. Specifically, the ion wave fluctuations exhibited a pronounced maximum (by several orders of mangitude) when $\Delta\omega = \underline{k}_S (c_S + \mu_O)$ where c_S is the ion acoustic frequency and μ_O the ion flow velocity ($\simeq$ 0.1-0.2 c_S depending upon ion species). In addition, the fluctuations scaled linearly with the magnitude of E_1 E_2 and were independent of the individual field amplitudes over two orders of magnitude variation. Finally, the density fluctuations were in quantitative agreement with the predictions of the analytic theory. when we investigated the region $v_O/v_{te} \simeq$ 0.1-0.25, we found in contrast a sharp nonlinear saturation at a level significantly below that predicted by the collision limited optical mixing theory. Interestingly, the saturated amplitude was $\simeq$ 5% as in the earlier microwave SBS studies. However, since the associated microwave power levels were approximatley an order of magnitude lower than in the pure SBS case there was no appreciable electron main body heating. In addition, no ion wave harmonics were observed. However, again there was strong ion tail heating as shown in Fig. 4. To demostrate the strong resonant nature of the heating process we varied the difference frequency as shown in the inset to Fig. 4. As in the SBS case, we obtain complete agreement between experimental results and numerical calculations which account for the ion tail heating.

2.2 Resonant self-focusing

Longitudinal electron plasma waves (EPW) of wavenumber $\underline{k}_p = \Delta\underline{k}$ can be resonantly driven if $\omega_{EPW} = \Delta\omega$. If the two EM

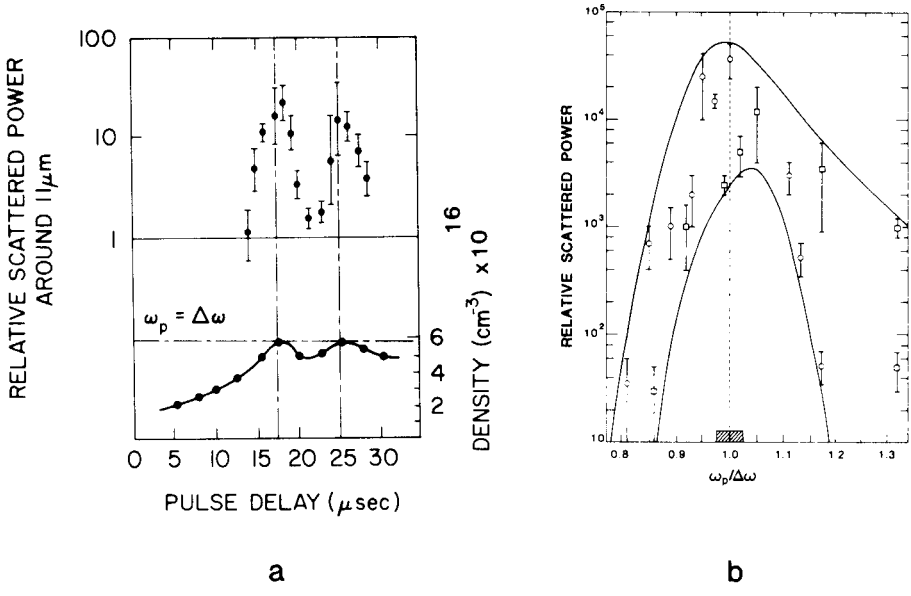

FIG.5. a) Time evolution of the arc density and scattered power in frequency $\omega_s = \omega(10.27\,\mu m) - \omega_p$; b) forward-refracted light in the 10.27-μm line versus $\omega_p/\Delta\omega$ with density measured by ruby interferometry (□) and by Stark broadening of a seed gas H_α line. The shaded areas indicate the spread of difference frequencies in the incident beam.

waves are colinear, then the phase velocity of the EPW, $v_p = \omega_{EPW}/k_p$, is ≃ the group velocity of the EM waves, $v_g = c(1-\omega_p^2/\omega_o^2)^{\frac{1}{2}}$; and the three waves are locked into synchronism over thousands of wavelengths if $\omega_p << \omega_o$. Also, since $v_p \simeq c$, there is little Landau damping; and the EPW can grow to a very large amplitude.

We have experimentally investigated the process [9] by focusing the 9.6-μm and 10.27-μm lines of the CO_2 laser to an intensity of 10^{10} W/cm^2 by an f/7.5 lens to a 300-μm spot in a preionized Ar arc plasma. The transmitted light plus any forward scattered light was collected by a Hg:Ge photoconductor. The evidence for optical mixing was obtained by the observation of a new line in the forward-scattered light around 11 μm which is produced by Thomson scattering of the 10.27-μm line from the EPW generated by the beat wave. Moreover, this radiation was only observed when $\Delta\omega = \omega_p$ as shown in Fig. 5a. Although the FWHM of the input laser pulse was 75-ns, the 11-μm line was only about 25-ns wide. Another unusual and at first puzzling effect was observed. Whenever $\Delta\omega = \omega_p$, very strong refraction of the beam occurred outside the cone angle of the incident beam (Fig. 5b). This phenomenon has been called resonant

FIG.6. Photograph of the density striations (centre of the picture) produced by the CO_2 laser beam in a 0.1-n_c plasma obtained by using optical Fourier transform techniques.

self-focusing due to the ponderomotive force the EPW. The ponderomotive force of the plasmon can be much larger than that of light. The amplification factor A is given by

$$A = \frac{F_{NL}(\text{plasmon})}{F_{NL}(\text{light})} = \left[\frac{-(\omega_p^2/\omega_o^2)\ \nabla\ \langle E_o^2\rangle/8\pi}{-\ \langle E_p^2\rangle/8\pi}\right]^{-1} = \frac{(\tilde{n}/n_o)^2}{(v_o/c)^2}$$

Using the value of $\tilde{n}/n_o \simeq 0.4\%$ estimated from the absolute levels of Thomson scattered light from the EPW and $I_o = 10^{10}$ W/cm^2, we obtain $A > 20$. Since the EPW wavelength is about the same as the focal spot diameter, the longitudinal and transverse gradients of the electric fields are comparable; and a density depression is created on axis which causes deflection of the beam by refraction. It is not clear whether the amplitude fo the EPW in this experiment was limited by relativistic effects or ion dynamics. However, the time duration of the EPW was almost certainly limited by ion motion. The wave potential corresponding to $\tilde{n}/n_o \simeq 0.4\%$ was about 2.5 kV (i.e. $<<$ mc2); and since T_e was only 5 eV, no hot electrons due to trapping were expected.

3. Filamentation

By using optical Fourier transform techniques, we have obtained photographs of plasma density striations in the focal region of a 350-MW CO_2 laser beam focused by an f/7.5 lens into a hydrogen plasma with density of 0.1 n_c. [10] An example is shown in Fig. 6. Density variations of 200 μm can be seen near the focus of the pump beam. The observed spatial frequency and the estimated density change imply that the striated regions are

also the regions of self-trapped radiation channels in which the individual beamlets are nondiffracting rather than self-focusing filaments.

4. Resonance Absorption (RA)

Phenomena at densities near critical can be studied in microwave experiments. we have specifically examined hot electron production and localized electric field generation associated with RA in a fixed density profile. At low intensities, the plasma wave saturation level agrees with convection out of the critical-density region; at high intensities, the saturation level follows cold-plasma wave-breaking scaling. The transition to wave-breaking saturation, however, occurs at power levels several orders below those predicted by the usual models. Finite pump bandwidth $\Delta\omega = \delta\omega_o$ was found, in the wave-breaking regime, to reduce the electric field E_b, the maximum electron energy ε_m, and the density n_h and temperature T_h of the hot electrons, and to increase the wave-breaking time τ_b as follows: $n_h \propto \delta^{-0.43}$, $T_h \propto \delta^{-0.31}$, $E_b \propto \delta^{-0.6}$, $\varepsilon_m \propto \delta^{-0.67}$, $\tau_b \propto \delta^{0.3}$. The last three of these agree with cold-plasma wave-breaking theory.[11]

REFERENCES

[1] J.J. TURECHEK and F.F. CHEN, Phys. Fluids, 24 (1981) 1126.

[2] M.J. HERBST, E.C. CLAYTON, and F.F. CHEN, J. Appl. Phys. 51 (1980) 4080.

[3] M.J. HERBST, E.C. CLAYTON, and F.F. CHEN, Phys. Rev. Letts. 43, (1981) 1591.

[4] C.E. CLAYTON, C. JOSHI, A. YASUDA, and F.F. CHEN, Phys. Fluids 24, (1981) 2312.

[5] C.E. CLAYTON, C. JOSHI, and F.F. CHEN, Bull. Am. Phys. Soc. 26 (1981) 933.

[6] D.W. FORSLUND, J.M. KINDEL, and E.L. LINDMAN, Phys. Fluids 18 (1975) 1002.

[7] H.E. HUEY, A. MASE, N.C. LUHMANN, JR., W.F. DiVERGILIO, and J.J. THOMSON, Phys. Rev. Lett. 45 (1981) 795.

[8] A. MASE, N.C. LUHMANN, JR., J. HOLT, H. HUEY, M. RHODES, W.F. DiVERGILIO, J.J. THOMSON, and C.J. RANDALL, Plasma Physics and Controlled Nuc. Fusion Res. IAEA, Vienna, II (1981) 745.

[9] C. JOSHI, C.E. CLAYTON, and F.F. CHEN, Phys. Rev. Lett. 48 (1981) 874.

[10] C. JOSHI, C.E. CLAYTON, A. YASUDA, and F.F. CHEN, J. Appl. Phys. 53 (1982) 215.

[11] A.Y. LEE, Y. NISHIDA, N.C. LUHMANN, JR., S.P. OBENSCHAIN, B. GU, M. RHODES, J.R. ALBRITTON, and E.A. WILLIAMS, Phys. Rev. Lett. 48 (1982) 319.